

Assembly of Colloidal Nanoparticles into Hollow Superstructures by Controlling Phase Separation in Emulsion Droplets

Chaolumen Wu, Zhenda Lu, Zhiwei Li, and Yadong Yin**

C. Wu, Dr. Z. Li, Prof. Y. Yin

Department of Chemistry, University of California, Riverside, CA 92521, USA

E-mail: yadong.yin@ucr.edu

Prof. Z. Lu

College of Engineering and Applied Science, Nanjing University, Nanjing, Jiangsu, 211816, P. R. China

E-mail: luzhenda@nju.edu.cn

Keywords: hollow superstructures, nanoparticle assembly, phase separation, emulsion

Template-mediated self-assembly of colloidal nanoparticles into secondary structures is of particular importance for exploring new materials with unique collective properties. However, the limited available templates and the poor control over the assembly of nanoparticles within the space defined by the templates drastically inhibit the preparation of the superstructures with the desired size and morphology. Here, a general method to prepare submicron hollow superstructures by self-assembling hydrophobic colloidal nanoparticles together with polymeric additives within oil-in-water emulsion droplets is reported. Upon evaporation of low boiling point oil, phase separation occurs to drive the assembly of nanoparticles at the polymer/water interface, producing a nanoparticle shell surrounding each polymeric core. Such core-shell structures can be converted into hollow superstructures of nanoparticles by stabilization with a silica coating and removal of the polymeric additives by solvent dissolution. Upon calcination, the silica layer can be further etched to release free-standing hollow shells of nanoparticles. With its general applicability to the assembly of various nanoparticles, this method represents a new platform for the fabrication of diverse hollow superstructures toward broad applications that can take advantage of the collective properties of the nanoparticles and the hollow morphology of the assemblies.

1. Introduction

Controlled assembly of nanoparticles into secondary structures opens new avenues to manufacture functional materials with tailored physical and chemical properties, which are highly desirable in many important applications ranging from catalysis to biological labeling and imaging, and drug encapsulation and delivery.^[1] Ligand-stabilized colloidal nanoparticles, predominantly prepared through thermolytic routes by reacting inorganic precursors in organic solvents at high temperatures, are ideal building blocks for assembly due to their narrow size distributions, well-protected surfaces, uniform shapes, and tunable properties.^[2] Moreover, the resulting nanoparticles typically possess a well-defined monolayer of capping ligands, which can be tuned to modulate their interactions with each other or with the surroundings.^[3] The self-assembly of colloidal nanoparticles into three-dimensional superstructures is of particular importance toward the fabrication of new devices with unique collective properties.^[4] Nanoparticles assembly based on an emulsion-evaporation method has been investigated as a way to synthesize three-dimensional superstructures.^[5] However, the assembled superstructures tend to pack closely and adopt spherical shapes to minimize the surface energy, and the desired crystal domains and crystal shapes are difficult to achieve during the nanoparticle assembly.^[6]

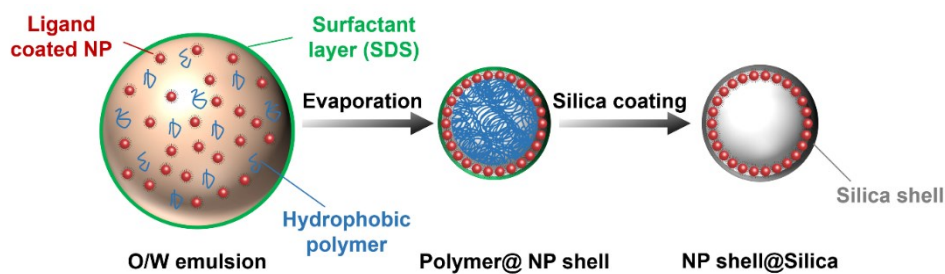
Self-assembled hollow superstructures are a distinct type of capsules with a shell of densely packed colloidal particles, featuring large surface areas, abundant active sites, large cavities, and low density.^[7] They can be produced by assembling colloidal nanoparticles on a sacrificial hard template such as silica, polystyrene, and carbon spheres and subsequently removing the template by calcination, etching, or decomposition. Although classic, hard templating is typically not suitable for large-scale production due to the requirement of pre-synthesized templates, which are usually expensive to make.^[8] The soft templating methods circumvent the problem by employing liquid droplets as templates and assembling nanoparticles at liquid-liquid interfaces,^[9] which, however, mainly produce relatively large hollow particles as limited

by the droplet size. It remains a challenge to be extended to submicron hollow structures, which are technologically important for many biomedical applications.^[10] In principle, uniform nanoparticles with diameters ranging from 2 to 50 nm are ideal candidates to assemble at the liquid-liquid interface to form hollow superstructures. However, at this length scale, the reduction in Helmholtz free energy diminishes, and detachment of particles from the liquid-liquid interface occurs due to thermal fluctuations.^[10a] Furthermore, the success of this method is also challenged by the difficulty in stabilizing the resulting hollow superstructures, although complex surface modification procedures have been explored to introduce reactive organic molecules to lock the nanoparticles in position.^[7, 11] On the other hand, template-free methods eliminate the need for templates and assemble nanoparticles into hollow superstructures through electrostatic interactions and dispersion and other forces like hydrogen bonding.^[8b, 12] For example, water-dispersible gold nanoparticles were assembled into spherical capsids with monolayer shells through hydrogen bonding between neighboring nanoparticles.^[13] Although straightforward, the assembly is typically limited to nanoparticles containing specific ligands, preventing its broad applicability.

Here, we report a novel and general method for preparing submicron hollow superstructures by manipulating the nanoparticle assemblies produced by evaporating emulsion droplets. While the emulsion evaporation method was initially developed for producing spherical superstructures,^[3b, 14] it was recently shown that phase separation might occur within the droplets to generate core-shell or Janus structures.^[15] In this work, we take advantage of the phase separation and demonstrate a general approach for creating hollow superstructures of colloidal nanoparticles by co-assembling them with polymer additives within emulsion droplets. As illustrated in Scheme 1, hydrophobic ligand-capped nanoparticles and hydrophobic polymers are first co-assembled into polymer/nanoparticle core-shell structures by the emulsion evaporation method. Upon the evaporation of the low boiling point solvent, phase separation

occurs to drive the assembly of nanoparticles at the polymer/water interface of the droplets, forming a layer of nanoparticles around each polymer core. The nanoparticle shells can be stabilized by a silica coating and then converted into hollow superstructures by removing the polymer core through solvent etching. This general method can be extended to nanoparticles of various materials to prepare submicron hollow superstructures with fine tunability of sizes and components.

2. Result and Discussion



Scheme 1. Schematic illustration of the preparation procedure for nanoparticle shell (NP shell).

We chose γ -Fe₂O₃ nanoparticles as the model system for this study because of their well-controllable sizes, good stability, and superparamagnetic properties. Uniform γ -Fe₂O₃ nanoparticles with sizes ranging from 5 to 20 nm were prepared by a thermolytic method using oleic acid (OA) as the capping ligand.^[16] In a typical process, 12.7-nm γ -Fe₂O₃ nanoparticles (5 mg) (shown in Figure 1a) together with a polymeric additive of poly(1-decene) (3 mg) were dispersed in cyclohexane, which was then emulsified in SDS aqueous solution to produce an O/W emulsion system. Upon the evaporation of the low boiling point cyclohexane at about 65 °C, the γ -Fe₂O₃ nanoparticles were excluded from the polymer phase due to their immiscibility and assembled on the interface of poly(1-decene)/water to form the nanoparticle shells (as shown in Scheme 1). The as-synthesized polymer/nanoparticle core-shell structures are relatively stable and can be stored in the aqueous solution for several days without obvious changes, but they will collapse upon deposition and drying on a solid substrate. To protect the assembled structures, they were coated with a thin layer of silica by modifying the well-known Stöber method.^[17] As shown in Figure 1b, a γ -Fe₂O₃ nanoparticle layer at the interface can be seen with the silica layer coated on the exterior of each nanoparticle shell.

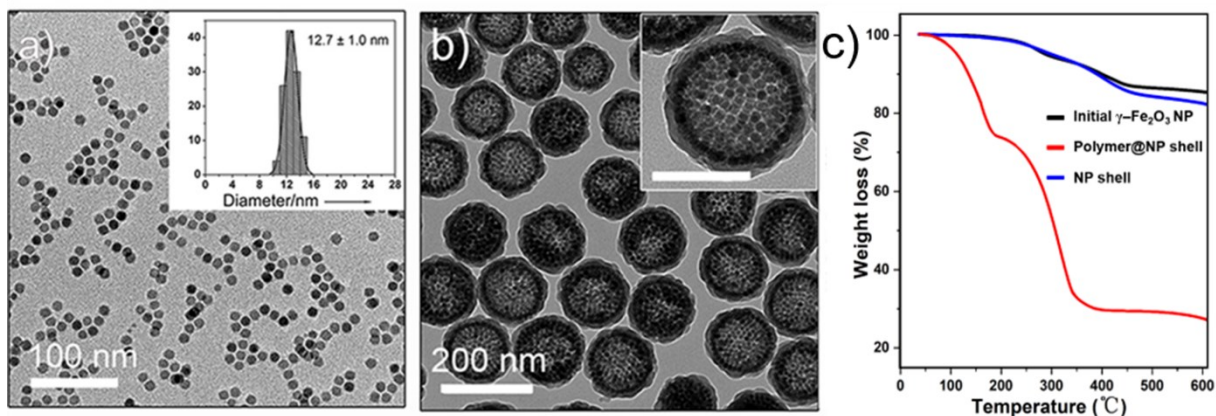


Figure 1. (a) TEM image of 12.7-nm γ -Fe₂O₃ nanoparticles. Inset is the size distribution of the 12.7-nm γ -Fe₂O₃ nanoparticles. (b) TEM image of silica-coated nanoparticle shells assembled using 3 mg poly(1-decene) and 5 mg of 12.7-nm γ -Fe₂O₃ nanoparticles. Inset is a high-magnification TEM image with a scale bar of 100 nm. (c) TGA curves of original γ -Fe₂O₃ nanoparticles, polymer@NP shells, and NP shells obtained after ethanol washing.

At the end of the silica coating process, the polymer cores could be dissolved by the solvent ethanol and diffuse through the porous silica shell to produce hollow superstructures. Thermogravimetric analysis (TGA) of the initial γ -Fe₂O₃ nanoparticles and their corresponding core-shell structures before and after ethanol washing revealed different weight loss profiles (Figure 1c). The evaporation of low boiling point solvent or trapped moisture in nanoparticles led to less than 5 wt% loss in the temperature range from 20 to 200 °C for both the initial nanoparticles and ethanol-washed nanoparticle shells. The weight loss in the same temperature range reached 22 wt% for the polymer@NP shells even after the sample was kept at 80 °C for 6 hours. The additional weight loss in the temperature range of 200-600 °C was mainly attributed to the evaporation and decomposition of organic substances, such as oleic acid, SDS, and poly(1-decene). The value of weight loss was about 18 wt% in the ethanol-washed nanoparticle shells, while in the core-shell sample, this value rose to 45 wt% due to the presence of the poly(1-decene). The obvious difference in weight loss before and after ethanol washing confirmed the removal of the polymer during ethanol washing.

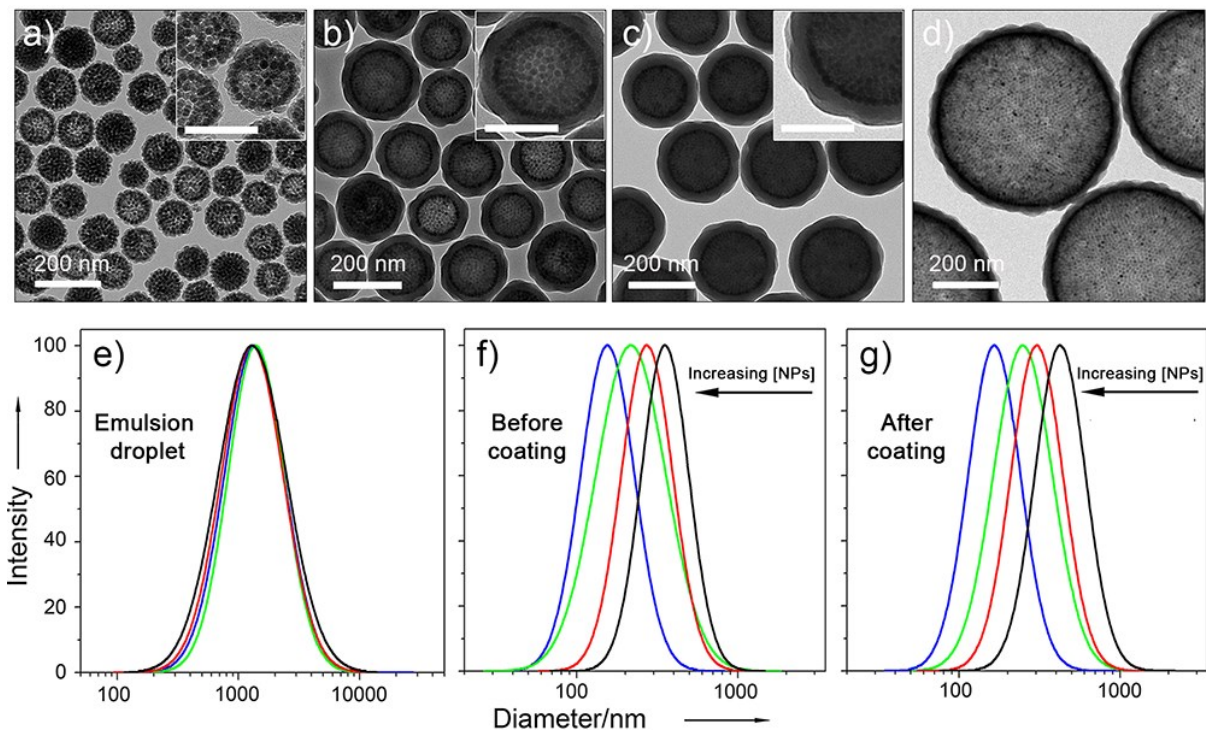


Figure 2. (a-c) TEM images of silica-coated nanoparticle shells assembled from poly(1-decene) (3 mg) and varying amounts of 12.7-nm γ -Fe₂O₃ nanoparticles: (a) 10 mg, (b) 2.5 mg, and (c) 1 mg. Insets are high-magnification TEM images with scale bars of 100 nm. (d) TEM image of silica-coated nanoparticle shells assembled from 5 mg of γ -Fe₂O₃ nanoparticles and 30 mg of poly(1-decene). (e-g) Size distribution of the emulsion droplets and corresponding nanoparticle shells assembled from 3 mg poly(1-decene) and different amount of nanoparticles: black (1 mg), red (2.5 mg), green (5 mg), and blue (10 mg), analyzed by dynamic light scattering (DLS): (e) emulsion droplets before solvent evaporation; (f) nanoparticle shells after solvent evaporation in a water bath (65 °C) for 4 h; (g) silica-coated nanoparticle shells.

To study the critical factors that influence the formation of hollow superstructures, we systematically varied the assembly parameters, including the ratio of the nanoparticles to polymer, the size of the γ -Fe₂O₃ nanoparticles, as well as the type of hydrophobic polymers. For nanoparticles with defined sizes, the diameter of the assembled nanoparticle shells can be tuned by controlling the mass ratio of γ -Fe₂O₃ nanoparticles to poly(1-decene). Figures 2a-c showed the TEM images of a series of silica-coated nanoparticle shells prepared by varying the

quantity of γ -Fe₂O₃ nanoparticles (12.7 nm) from 1 to 10 mg while using the same amount of poly(1-decene) (3 mg). Figure 2d exhibited another sample prepared with a further reduced nanoparticle/polymer ratio. Since it became difficult to collect products when the amount of nanoparticles is less than 1 mg, the sample was prepared by mixing 5 mg of γ -Fe₂O₃ nanoparticles and 30 mg of poly(1-decene). The sizes of the structures assembled using the same amount of poly(1-decene) were characterized by the DLS method. Figure 2e showed that the average sizes and distributions of the initial emulsion droplets were almost the same under different nanoparticle/polymer ratios. The mean diameters of the initial emulsion droplets were around 1.2 μ m. The average size of the emulsions shrunk to several hundred nanometers after evaporation of cyclohexane, with exact sizes determined by the remaining amounts of γ -Fe₂O₃ nanoparticles and poly(1-decene). The nanoparticle shell size increased as the γ -Fe₂O₃ nanoparticle content decreased from 10 to 1 mg, allowing a tuning range of 120 to 420 nm (Figure 2f). Silica coating slightly increased the average size of the corresponding shells, as suggested by the DLS measurements (Figure 2g). When the relative amount of polymer to nanoparticles was too small, the polymer cannot be evenly distributed among the emulsion droplets during emulsification, leading to a large variation in the thickness of the resulting nanoparticle shells (Figure 2a). On the other hand, the thickness of the silica layer decreased from 40 to less than 10 nm as the number of γ -Fe₂O₃ nanoparticles increased while adding the same amount of tetraethyl orthosilicate (TEOS). Therefore, it is reasonable to conclude that more nanoparticle shells were produced before coating and that more γ -Fe₂O₃ nanoparticles led to smaller shells. Although the actual nanoparticle and polymer concentrations were different from the other four samples, the one in Figure 2d had the largest shell size among all, with average diameters above 600 nm, further confirming the determining role of nanoparticle/polymer ratio. It is also worth noting that the nanoparticles tend to assemble in a short-range-ordered close-packing structure in the shells.

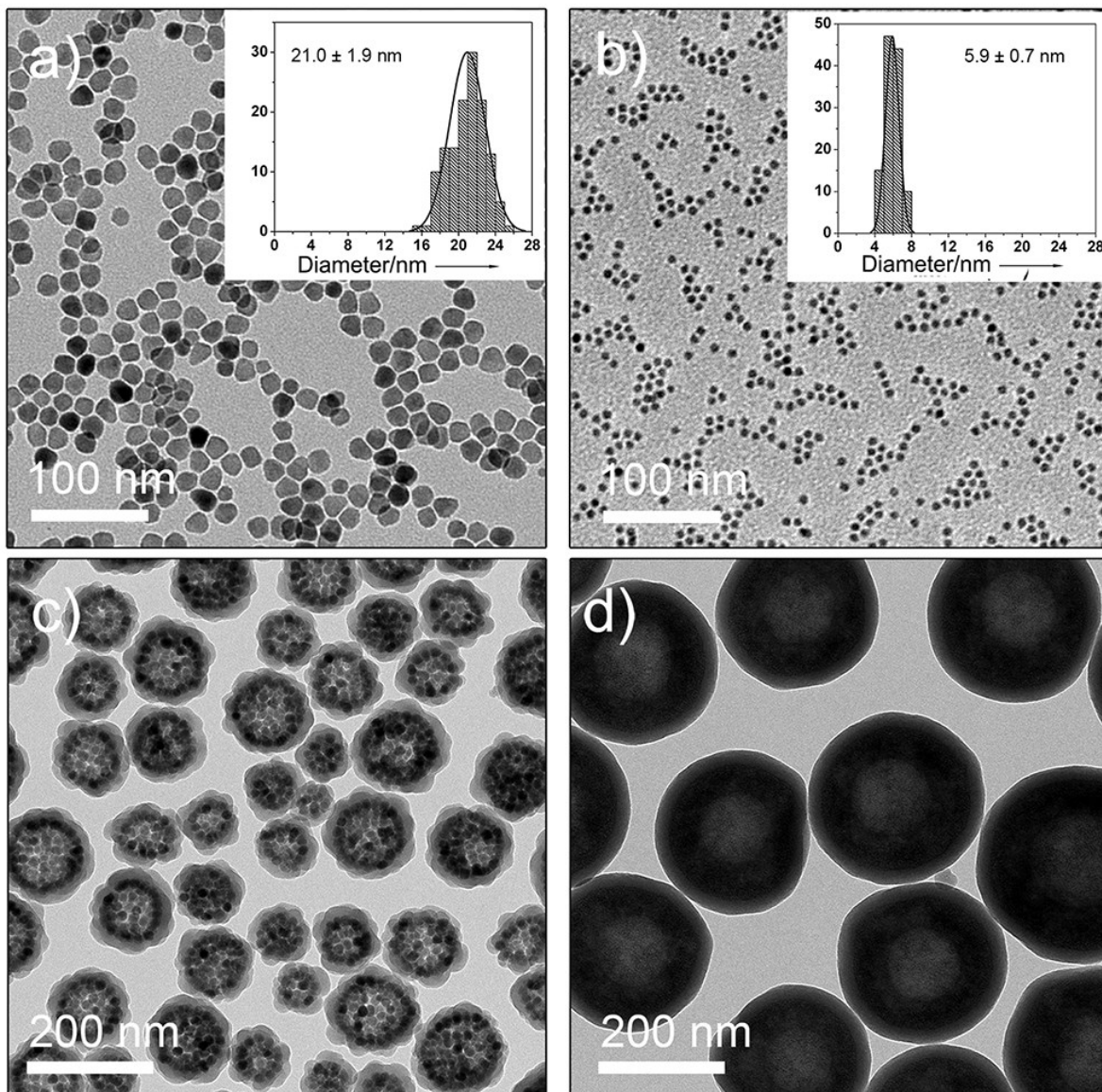


Figure 3. TEM images of (a) 21-nm and (b) 5.9-nm γ -Fe₂O₃ nanoparticles and the corresponding silica-coated nanoparticle shells assembled with poly(1-decene) (3 mg) and nanoparticles with different amounts: (c) 10 mg of 21-nm nanoparticles, (d) 2.5 mg of 5.9-nm nanoparticles. Insets in (a) and (b) are the size distribution of 21-nm and 5.9-nm nanoparticles.

The interfacial assembly of nanoparticles here, which is similar to Pickering emulsions,^[10a, 18] is driven by a decrease of total free energy (ΔE). The three contributions to the interfacial energy include the particle-oil interface energy ($\gamma_{P/O}$), the particle-water interface energy ($\gamma_{P/W}$), and the oil-water interface energy ($\gamma_{O/W}$). The energy difference (ΔE) due to the assembly of a single particle at the oil-water interface can be given by

$$\Delta E = -\frac{\pi r^2}{\gamma_{O/W}} \times (\gamma_{O/W} + \gamma_{P/O} - \gamma_{P/W})^2 ,$$

where r is the effective radius of the nanoparticle.^[10a] Based on published values for $\gamma_{O/W}$ of 52 mN/m,^[19] and on estimates for $\gamma_{P/O}$ of 40 mN/m (nanoparticles cannot be dispersed in poly(1-decene) at all) and for $\gamma_{P/W}$ of 15 mN/m (after SDS adsorption, the particles can be well dispersed in the water phase),^[9] ΔE is about $-3500 \text{ k}_\text{B}T$ for 12.7-nm nanoparticles in a typical poly(1-decene)/water emulsion. The energy gain is much larger than thermal energy (a few $\text{k}_\text{B}T$), which leads to effective confinement of nanoparticles at the interface. In a typical emulsion system, the total energy difference after assembly is determined by the square of the particle radius r because $\gamma_{P/O}$, $\gamma_{P/W}$, and $\gamma_{O/W}$ are constant. Therefore, the self-assembly of smaller nanoparticles is expected to be less stable than larger ones. To study the dependence of the assembled shells on nanoparticle size, we chose $\gamma\text{-Fe}_2\text{O}_3$ nanoparticles with three different sizes: 21.0, 12.7, and 5.9 nm. Because the maximum cross-section area of nanoparticle per mass unit is inversely proportional to the particle size, we used 10, 5, and 2.5 mg of $\gamma\text{-Fe}_2\text{O}_3$ nanoparticles for the 21.0-nm, 12.7-nm, and 5.9-nm nanoparticles, respectively, to ensure the same degree of nanoparticle coverage. Figure 1a, b and Figure 3 presented TEM images of the $\gamma\text{-Fe}_2\text{O}_3$ nanoparticles and corresponding silica-coated nanoparticle shells. Larger nanoparticles (21.0 and 12.7 nm) can be tightly fixed at the interface in a near-monolayer structure (Figure 3c and Figure 1b). The average size of the shells assembled from 21.0-nm nanoparticles was smaller than those assembled from 12.7-nm nanoparticles, indicating that the larger particles have a stronger stabilization effect for the assembly as predicted by the equation. However, as the small nanoparticles have a relatively small energy decrease upon self-assembly, the 5.9-nm $\gamma\text{-Fe}_2\text{O}_3$ nanoparticles formed relatively thick shells at the interface to stabilize the polymer droplets in the system (Figure 3d). The effect of the mass ratio of the nanoparticle to polymer for 5.9-nm and 21.0-nm $\gamma\text{-Fe}_2\text{O}_3$ nanoparticles was also studied and showed the same result as the 12.7-nm sample. In Figure 3d and Figure S1a, b, different amounts (2.5, 5.0, and 1.0, mg)

of γ -Fe₂O₃ nanoparticles (5.9 nm) were mixed with a fixed amount of poly(1-decene) (3 mg) and assembled into nanoparticle shells. Small γ -Fe₂O₃ nanoparticles were assembled into multilayer shells, and the size of the nanoparticle shells increased as the number of γ -Fe₂O₃ nanoparticles decreased. For large γ -Fe₂O₃ nanoparticles (21 nm) (shown in Figure 3c and Figure S1c, d), they were assembled into small near-monolayer shells with similar dependence of shell size on the nanoparticle amount.

In addition to the nanoparticle size, the wettability of the particle surface is also related to the free energy and subsequently affects the nanoparticle assembly on the interface. In the above equation, the values of $\gamma_{O/W}$ and $\gamma_{P/O}$ can be tuned by using different oil phases (hydrophobic polymers). Obviously, larger $\gamma_{O/W}$ and $\gamma_{P/O}$ values should produce a more stable interfacial assembly. 1-octadecene (ODE), hydrogenated poly(1-decene), and polystyrene (Mw=192000) were chosen to study the assembly behavior, and the TEM results were shown in Figure S2. 1-octadecene and hydrogenated poly(1-decene), with lower $\gamma_{O/W}$ and $\gamma_{P/O}$ values than poly(1-decene), cannot promote the effective assembly of nanoparticles at the interface, while polystyrene with a large molecular weight can easily serve as a rigid template to form a well-defined nanoparticle shell. Although polystyrene (Mw=192000) has a high molecular weight, it could still diffuse out after the silica-coated nanoparticle shells were stored in ethanol for 1 week, leading to hollow superstructures (Figure S3).

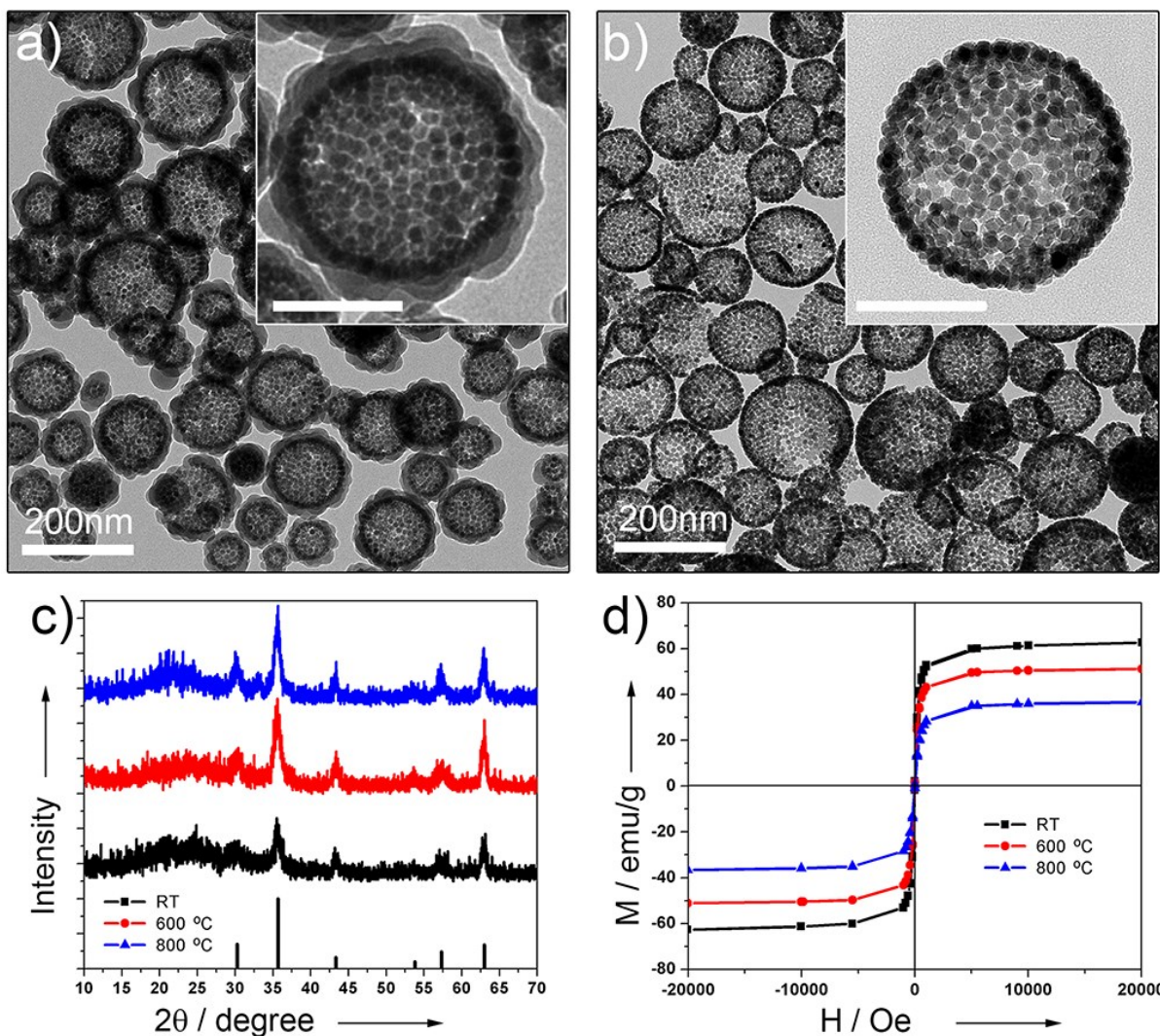


Figure 4. (a) TEM images of silica-coated nanoparticle shells. (b) TEM images of nanoparticle shells after calcination at 800 °C for 2 hours and silica removal. Insets are high-magnification TEM images with scale bars of 100 nm. (c) X-ray diffraction patterns and (d) magnetization hysteretic loops of the three nanoparticle shells after different calcination temperatures. The JCPDS card No. for pure γ -Fe₂O₃ used in (c) is 39-146.

Fixing the nanoparticles inside the superstructures by calcination produces robust and water-dispersible nanoparticle shells, which are stable even after removing the protecting layers. A silica coating was introduced to the nanoparticle shells to maintain the assembled structure (Figure 4a) and allow the neighboring nanoparticles to build atomic interconnection during calcination. Final etching of silica after calcination introduces high-density hydroxyl groups so

that the nanoparticle shells become negatively charged and can disperse well in water. To partially fuse the nanoparticles in the shell while maintaining the morphology and properties, we tested different calcination temperatures from 300 °C to 800 °C. As shown in Figure S4a-c, without calcination or after low-temperature calcination (below 500 °C), the nanoparticle shells were disassembled into single nanoparticles or irregular aggregations after the removal of silica. Calcination at 500 °C induced some fusion between nanoparticles to form stable shells, but only with a low yield. Temperatures above 600 °C were suitable for linking neighboring γ -Fe₂O₃ nanoparticles (shown in Figure S4d-f). Figure 4b showed intact hollow superstructures of γ -Fe₂O₃ nanoparticles after calcination at 800 °C and silica removal. Without protection, γ -Fe₂O₃ nanoparticles would aggregate and be transformed to the antiferromagnetic hematite α -Fe₂O₃ phase above a certain temperature,^[20] typically around 400 °C (Figure S5). In contrast, the silica-coated γ -Fe₂O₃ hollow superstructures exhibited enhanced thermal stability, with samples calcined at different temperatures consisting primarily of the maghemite γ -Fe₂O₃ (JCPDS Card No. 39-1346) with almost identical peak broadening, as shown in the XRD analysis in Figure 4c. In this case, all the samples were etched by a sodium hydroxide solution to eliminate the influence of silica before characterization. The primary nanocrystals did not grow significantly during the self-assembly and calcination. The slight increase in grain size of the calcined samples suggested a possible interparticle fusion, which contributed to the formation of stable hollow superstructures. The corresponding room-temperature magnetization curves in Figure 4d revealed the superparamagnetic behavior of all three samples. We noted that after calcination at 800 °C, a small peak corresponding to the hematite phase appeared on the XRD pattern, and the saturation magnetization value decreased from 63 to 37 emu/g, suggesting a partial transformation from maghemite to hematite phase. However, the as-synthesized hollow superstructures still exhibited superparamagnetic properties even after treatment at 800 °C. Thus, they can be magnetically separated from the colloidal dispersion. These results implied that the SiO₂ shells not only stabilized the nanoparticle shells during calcination but also

inhibited the phase transition of γ -Fe₂O₃ to α -Fe₂O₃ and maintained the superparamagnetic property of the nanocrystals.

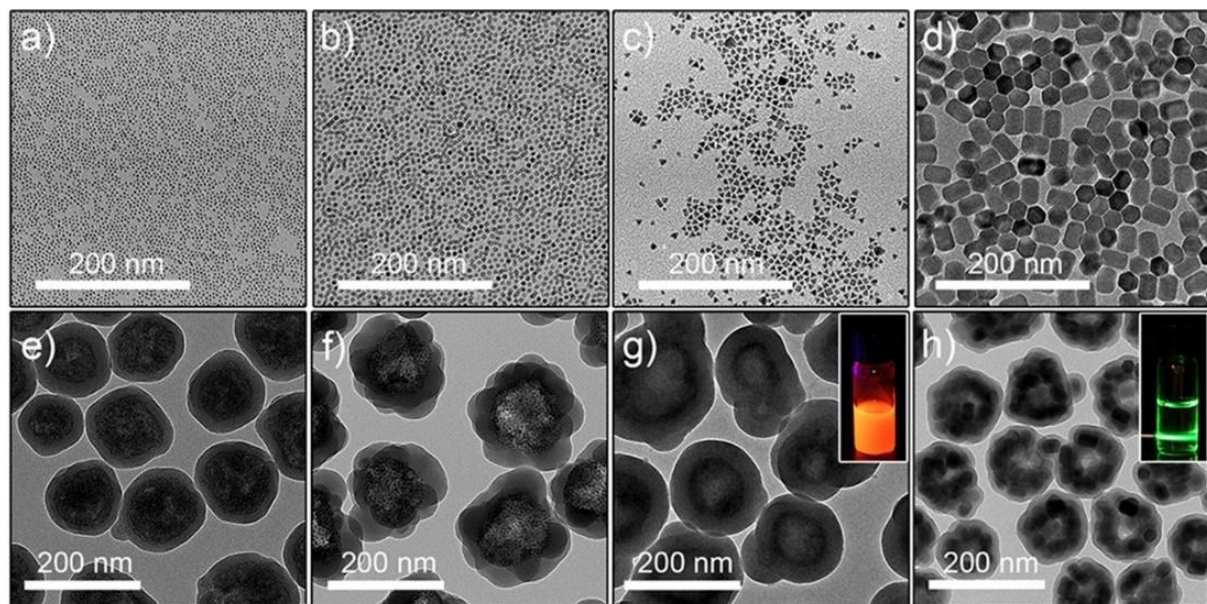


Figure 5. TEM images of different nanoparticles (a, b, c and d) and corresponding silica-coated nanoparticle shells (e, f, g and h): (a, e) ZrO₂, (b, f) NiO, (c, g) CdSe@CdZnS (QDs), (d, h) NaYF₄:Yb,Er. Insets are digital photos of the aqueous dispersions of (g) CdSe@CdZnS nanoparticle shells excited by an ultraviolet lamp, (h) NaYF₄:Yb,Er nanoparticle shells excited by a 980-nm laser.

Nanoparticle assembly at the polymer/water interface is a general and flexible approach for producing stable hollow superstructures from nanoparticles of various compositions. To test the versatility of the assembly process, various hydrophobic nanoparticles, including trioctylphosphine oxide-capped ZrO₂,^[21] oleylamine-capped NiO,^[22] oleic acid-capped CdSe@CdZnS^[23] and oleic acid-capped NaYF₄:Yb,Er^[24] were assembled at the poly(1-decene)/water interface. As shown in Figure 5, they were all assembled into hollow superstructures, indicating the versatility of the assembly strategy. Similar to the γ -Fe₂O₃ nanoparticles, the small ZrO₂ nanoparticles (~4 nm) and the QDs (~6 nm) prefer to form multi-layered hollow superstructures at the poly(1-decene)/water interface (Figure 5 e, f). Conversely,

the larger NiO (~ 8 nm) and NaYF₄ ($\sim 30 \times 50$ nm) nanoparticles tend to form well-defined shells (Figure 5 g, h). It is worth noting that after the assembly, the QDs and NaYF₄:Yb,Er nanoparticles still exhibited good photoluminescence properties (shown in insets of Figure 5 g, h).

3. Conclusion

In summary, we report a general strategy for the fabrication of submicron hollow superstructures by controlling the phase separation of nanoparticles from polymer additives confined within emulsion droplets. The size and shell thickness of the hollow superstructures can be conveniently tuned by controlling the nanoparticle/polymer ratio in the oil droplets, the size of the nanoparticles, and the type of polymer additives. The resulting hollow superstructures can be further stabilized by overcoating a layer of silica followed by high-temperature calcination, producing water-dispersible free-standing nanoparticle shells after chemical etching of the silica. This assembly approach is expected to provide the research community with a highly versatile, configurable, and reproducible process to prepare submicron hollow superstructures of various nanoparticle building blocks, offering new opportunities to explore applications that can take advantage of the collective properties of the nanoparticles and the hollow morphology of the superstructures.

4. Experimental Section

Synthesis of γ -Fe₂O₃ nanoparticles: Superparamagnetic γ -Fe₂O₃ nanoparticles were synthesized using a thermolysis process.^[25] Fe(CO)₅ (0.2 mL, 1.52 mmol) was added to a mixture containing 10 mL of octyl ether and 1.28 g of oleic acid at 100 °C. The solution was then heated to 290 °C under the argon atmosphere and maintained at this temperature for 1 hour. After cooling down to 200 °C, the solution was bubbled with air for 2 hours. After cooling down to room temperature, ethanol was added to the solution to precipitate γ -Fe₂O₃ nanoparticles, which were

then separated by centrifugation. Finally, the resulting black powder was redispersed in cyclohexane.

Synthesis of CdSe@CdZnS nanoparticles (QDs): CdSe@CdZnS nanoparticles were prepared by a reproducible method reported by the Dubertret group.^[23] First, four reagents were prepared exactly based on the reference: (1) cadmium myristate, (2) Cd(oleate)₂ 0.5 M in oleic acid, (3) Zn(oleate)₂ 0.5 M in oleic acid, and (4) TOPS 0.5 M solution in trioctylphosphine (TOP). Later, 1-octadecene (16 mL), cadmium myristate (170 mg), and selenium (12 mg) were mixed in a flask and kept at room temperature under vacuum for 1 hour. After that, the solution was heated up to 240 °C under the argon atmosphere and aged for 10 minutes, followed by the injection of 1 mL of oleic acid and waiting a further 2 minutes. After cooling the solution down to room temperature, the CdSe nanoparticles were precipitated by adding excess ethanol and then harvested by centrifugation. The resulting powder was redispersed in 10 mL of chloroform as a CdSe stock solution. CdZnS shell coating: trioctylamine (8 mL), CdSe stock solution (2 mL), Zn(oleate)₂ stock solution (400 μL) and Cd(oleate)₂ stock solution (200 μL) were mixed in a flask. Then, the mixture was degassed under vacuum for 1 hour and heated to 300 °C under the argon atmosphere. A mixture of 4.4 mL of trioctylamine and 0.6 mL of TOPS was slowly added to the hot solution using a syringe pump at the rate of 10 mL h⁻¹. The final solution was kept at 300 °C for 2 hours. The core/shell CdSe@CdZnS nanoparticles were precipitated by ethanol and finally dispersed in cyclohexane.

Synthesis of ZrO₂ nanoparticles: ZrO₂ nanoparticles were prepared by a non-hydrolytic solution-based reaction.^[21] trioctylphosphine oxide (TOPO) (10 g) was heated at 150 °C for 30 minutes under vacuum. After cooling the solution temperature to 60 °C under the N₂ atmosphere, zirconium (IV) isopropoxide propanol complex (1.56 g) and ZrCl₄ (1.16 g) were added into the solution. The resulting mixture was then heated to 340 °C and further heated for 2 hours at 340 °C to ensure a complete reaction. After cooling the system down to 80 °C, 20

mL of acetone was added to yield a white precipitate, which was isolated by centrifugation and subsequently washed with a cyclohexane/acetone mixture to remove extra surfactant. The resulting powder was redispersed in cyclohexane.

Synthesis of NaYF₄:Yb,Er nanoparticles: Upconversion fluorescent NaYF₄:18%Yb, 2%Er nanoparticles were synthesized according to a reference.^[24] YCl₃·6H₂O (242.7 mg), YbCl₃·6H₂O (70.0 mg), and ErCl₃·6H₂O (7.6 mg) were dissolved in 2 mL of methanol first and then mixed with oleic acid (6 mL) and 1-octadecene (15 mL) in a 100 mL three-neck flask. The solution was degassed at 150 °C under Argon for 30 min and then cooled down to room temperature. 10 mL of a methanol solution containing NaOH (0.1 g) and NH₄F (0.1481 g) were added and stirred for 30 minutes. After that, the solution was slowly heated to 110 °C and kept at 110 °C for 30 minutes to remove methanol and a small amount of water. During this period, one neck of the flask was left open under the flow of Argon. Then, the solution was quickly heated to 320 °C and aged for 1 hour under argon protection. After the solution was cooled down, acetone was added to precipitate the nanoparticles. The final NaYF₄:Yb,Er nanoparticles were redispersed in cyclohexane after washing with cyclohexane/acetone two times.

Synthesis of NiO nanoparticles: The NiO nanoparticles were synthesized by the hot injection method, according to a previous report.^[22] Typically, triphenylphosphine (5 g) was heated at 120 °C for 30 minutes under vacuum, and then the temperature was increased to 230 °C under the argon atmosphere. After that, a mixture of nickel (acetylacetonate)₂ (0.5 g) and oleylamine (2 mL) was quickly injected, and the solution was aged for 20 minutes. After cooling down to 160 °C, the solution was bubbled with air for 1 hour. Ethanol was added to the solution to precipitate NiO nanoparticles, which were then retrieved by centrifugation. The final black powder was redispersed in cyclohexane after washing two times.

Assembly of nanoparticles at polymer/water interface: The nanoparticle shells were assembled in emulsion oil droplets by evaporating the low-boiling-point solvent (the oil phase). In a typical experiment, 1 mL of a cyclohexane solution of nanoparticles (5 mg) was completely mixed with poly(1-decene) (3 mg) by sonication in an ultrasonic cleaner for 10 min and then added into an aqueous solution of SDS (56 mg SDS completely dissolved in 10 mL of H₂O by sonication for 3 min) in 20 mL glass vial, followed by sonication for 4 min. The mixture was then heated to 65 °C in a water bath for 4 hours. After that, the reaction solution was cooled down to room temperature. The final products were washed with water one time and redispersed in 3 mL of water.

Silica coating/calcination/silica removal for nanoparticle shells: The nanoparticle shells were coated with a layer of SiO₂ by using a modified Stöber process. Typically, the above aqueous solution of nanoparticle shells (3 mL) was first mixed with ethanol (20 mL) and ammonium hydroxide (1 mL, 28%) an aqueous solution. Then tetraethyl orthosilicate (TEOS) (30 µL) was injected into the solution and reacted for 20 min under vigorous stirring. The core/shell superstructures were collected by centrifugation and washed with ethanol three times. After drying under vacuum overnight, the precipitate was heated to 600 °C for 2 hours in air using a heating rate of 5 °C min⁻¹ to remove organic agents. Then the calcined particles were dispersed in NaOH aqueous solution (1 M) for 3~4 hours under stirring to remove the silica shell. The final nanoparticle shells were collected by centrifugation and washed with distilled water several times.

Supporting Information

Supporting Information is available from the Wiley Online Library or from the author.

Acknowledgements

We are grateful for the financial support from the U.S. National Science Foundation (DMR-1810485). Z.L. acknowledges the support from the National Natural Science Foundation of China (No.22075128)

Received: ((will be filled in by the editorial staff))

Revised: ((will be filled in by the editorial staff))

Published online: ((will be filled in by the editorial staff))

References

[1] a) Z. Lu, C. Gao, Q. Zhang, M. Chi, J. Y. Howe, Y. Yin, *Nano Lett* **2011**, *11*, 3404; b) D. V. Talapin, J.-S. Lee, M. V. Kovalenko, E. V. Shevchenko, *Chem. Rev* **2010**, *110*, 389; c) M. V. Kovalenko, L. Manna, A. Cabot, Z. Hens, D. V. Talapin, C. R. Kagan, V. I. Klimov, A. L. Rogach, P. Reiss, D. J. Milliron, P. Guyot-Sionnest, G. Konstantatos, W. J. Parak, T. Hyeon, B. A. Korgel, C. B. Murray, W. Heiss, *ACS Nano* **2015**, *9*, 1012; d) Z. Li, W. Wang, Y. Yin, *Trends Chem.* **2020**; e) Z. Li, F. Yang, Y. Yin, *Adv. Funct. Mater* **2020**, *30*, 1903467; f) Z. Li, Y. Yin, *Adv. Mater* **2019**, *31*, 1807061.

[2] a) Y. Yin, A. P. Alivisatos, *Nature* **2005**, *437*, 664; b) S. Yin, Z. Li, L. Cheng, C. Wang, Y. Liu, Q. Chen, H. Gong, L. Guo, Y. Li, Z. Liu, *Nanoscale* **2013**, *5*, 12464.

[3] a) H. Skaff, Y. Lin, R. Tangirala, K. Breitenkamp, A. Böker, T. P. Russell, T. Emrick, *Adv. Mater* **2005**, *17*, 2082; b) J. Zhuang, H. Wu, Y. Yang, Y. C. Cao, *J. Am. Chem. Soc.* **2007**, *129*, 14166.

[4] a) T. Wang, D. LaMontagne, J. Lynch, J. Zhuang, Y. C. Cao, *Chem. Soc. Rev* **2013**, *42*, 2804; b) W. Xu, Z. Li, Y. Yin, *Small* **2018**, *14*, 1801083.

[5] F. Bai, D. Wang, Z. Huo, W. Chen, L. Liu, X. Liang, C. Chen, X. Wang, Q. Peng, Y. Li, *Angew. Chem. Int. Edit.* **2007**, *46*, 6650.

[6] Z. Yang, T. Altantzis, D. Zanaga, S. Bals, G. V. Tendeloo, M.-P. Pileni, *J. Am. Chem. Soc.* **2016**, *138*, 3493.

[7] Z. Xue, P. Wang, A. Peng, T. Wang, *Adv. Mater* **2019**, *31*, 1801441.

[8] a) F. Caruso, R. A. Caruso, H. Möhwald, *Science* **1998**, *282*, 1111; b) Z. Xue, P. Wang, A. Peng, T. Wang, *Adv. Mater* **2019**, *31*, 1801441.

[9] Y. Lin, H. Skaff, T. Emrick, A. D. Dinsmore, T. P. Russell, *Science* **2003**, *299*, 226.

[10] a) T. Bollhorst, K. Rezwan, M. Maas, *Chem. Soc. Rev* **2017**, *46*, 2091; b) A. Dinsmore, M. F. Hsu, M. Nikolaides, M. Marquez, A. Bausch, D. Weitz, *Science* **2002**, *298*, 1006; c) T.

Joki, M. Machluf, A. Atala, J. Zhu, N. T. Seyfried, I. F. Dunn, T. Abe, R. S. Carroll, P. M. Black, *Nat. Biotechnol* **2001**, *19*, 35.

[11] J. T. Russell, Y. Lin, A. Böker, L. Su, P. Carl, H. Zettl, J. He, K. Sill, R. Tangirala, T. Emrick, K. Littrell, P. Thiagarajan, D. Cookson, A. Fery, Q. Wang, T. P. Russell, *Angew. Chem. Int. Edit.* **2005**, *44*, 2420.

[12] a) J. S. Haataja, J. V. Timonen, S. Malola, P. Engelhardt, N. Houbenov, M. Lahtinen, H. Häkkinen, O. Ikkala, *Angew. Chem. Int. Edit.* **2017**, *56*, 6473; b) O. Ikkala, *Adv. Funct. Mater* **2018**, *28*, 1704328.

[13] T. Lahtinen, J. S. Haataja, T. R. Tero, H. Häkkinen, O. Ikkala, *Angew. Chem. Int. Edit.* **2016**, *55*, 16035.

[14] a) F. Bai, D. Wang, Z. Huo, W. Chen, L. Liu, X. Liang, C. Chen, X. Wang, Q. Peng, Y. Li, *Angew. Chem.* **2007**, *119*, 6770; b) J. Zhuang, H. Wu, Y. Yang, Y. C. Cao, *Angew. Chem. Int. Edit.* **2008**, *47*, 2208.

[15] a) T. Isojima, S. K. Suh, J. B. Vander Sande, T. A. Hatton, *Langmuir* **2009**, *25*, 8292; b) L. Zhang, Q. Fan, X. Sha, P. Zhong, J. Zhang, Y. Yin, C. Gao, *Chem. Sci* **2017**, *8*, 6103.

[16] J. Park, K. An, Y. Hwang, J.-G. Park, H.-J. Noh, J.-Y. Kim, J.-H. Park, N.-M. Hwang, T. Hyeon, *Nat. Mater* **2004**, *3*, 891.

[17] W. Stöber, A. Fink, E. Bohn, *J. Colloid Interface Sci.* **1968**, *26*, 62.

[18] K. L. Thompson, M. Williams, S. P. Armes, *J. Colloid Interface Sci.* **2015**, *447*, 217.

[19] C. Vasile, *Handbook of polyolefins*, CRC Press, **2000**.

[20] F. S. Yen, W. C. Chen, J. M. Yang, C. T. Hong, *Nano Lett* **2002**, *2*, 245.

[21] J. Joo, H. B. Na, T. Yu, J. H. Yu, Y. W. Kim, F. Wu, J. Z. Zhang, T. Hyeon, *J. Am. Chem. Soc.* **2003**, *125*, 11100.

[22] J. Park, E. Kang, S. U. Son, H. M. Park, M. K. Lee, J. Kim, K. W. Kim, H. J. Noh, J. H. Park, C. J. Bae, *Adv. Mater* **2005**, *17*, 429.

[23] O. Carion, B. Mahler, T. Pons, B. Dubertret, *Nat. Protoc* **2007**, *2*, 2383.

- [24] Z. Li, Y. Zhang, S. Jiang, *Adv. Mater.* **2008**, *20*, 4765.
- [25] T. Hyeon, S. S. Lee, J. Park, Y. Chung, H. B. Na, *J. Am. Chem. Soc.* **2001**, *123*, 12798.

A general strategy is developed for the fabrication of submicron hollow superstructures by controlling the phase separation of nanoparticles from polymer additives confined within an oil-in-water emulsion droplet. The resulting hollow superstructures can be further stabilized by calcination, producing water-dispersible free-standing hollow superstructures.

Chaolumen Wu, Zhenda Lu,* Zhiwei Li, and Yadong Yin*

Assembly of Colloidal Nanoparticles into Hollow Superstructures by Controlling Phase Separation in Emulsion Droplets

